LOAD-PATH AND STIFFNESS DEGRADATION OF FLOOR DIAPHRAGMS IN REINFORCED CONCRETE BUILDINGS SUBJECTED TO LATERAL LOADING

PART I: EXPERIMENTAL OBSERVATIONS

Parr, M.[1], Büker, F.[2], De Francesco, G.[1], Bull, D. K.[3], Brooke, N.[4], Elwood, K. J. [2], Hogan, L.[2], Liu, A.[5], Sullivan,T. [1]

ABSTRACT

An experimental investigation into the degradation of load-paths in damaged diaphragms was conducted to provide answers to the New Zealand structural engineering community following concerns that strut-and-tie load-paths could not cross wide cracks that develop around the floor perimeter during earthquake loading demands. A full-scale super-assembly concrete moment frame specimen with a hollow-core flooring system installed was subjected to realistic drift deformations to induce damage in the floor, followed by in-plane shear deformation demands to assess the ability of the diaphragm to transfer load between frames at different floor damage levels. It was found that compression struts could form across much wider cracks in floors than previously anticipated. This was due to contact compressive stresses forming via loose aggregate that lodged within rugged sinusoidal wide floor cracks. Additionally, it was found that diaphragm compression struts can only transfer to the primary lateral load resisting frame through beam plastic hinges acting in minor axis shear following gaps opening between the floor and columns at moderate drift demands. Smooth floor to column interfaces did not provide the same residual rubble aggregate binding compressive load path observed in cracks within the floor. The primary driver of diaphragm shear stiffness degradation was found to be torsional softening of the perimeter beams of the floor. This was caused by simultaneous bi-directional demands applied to longitudinal beam bars and a phenomenon known as the bowstring effect applying large torsional demands through the beam-floor continuity reinforcement. The diaphragm strength and rate of shear stiffness degradation was found to be highly reliant on earthquake directionality. A set of generalised equations was developed to describe the rate of diaphragm shear stiffness degradation with respect to magnitude and directionality of drift demands.

Part I of II in this journal series details the full-scale super-assembly experiment conducted on a floor diaphragm at different damage states and the observed behaviour during testing.

1 INTRODUCTION AND OBJECTIVES

The purpose of a floor diaphragm is to link frame and lateral load resisting elements to stiffen a structure subjected to lateral loading, such as earthquake demands. In design a rigid diaphragm assumption is typically used, meaning it is assumed the frames are perfectly linked through the floor for the entirety of lateral loading. The strut-and-tie method is generally used to identify and design load-paths for floor diaphragms (SNZ 2017). This method is used to understand the flow of internal forces for many aspects of reinforced concrete design and assumes that all compression forces are borne through the concrete in compression “struts” and all tension forces are transferred through steel reinforcing acting as tension “ties”. Concrete is assumed to carry no tension and steel is assumed to carry no compression. Examples of typical strut-and-tie solutions are displayed in Figure 1.

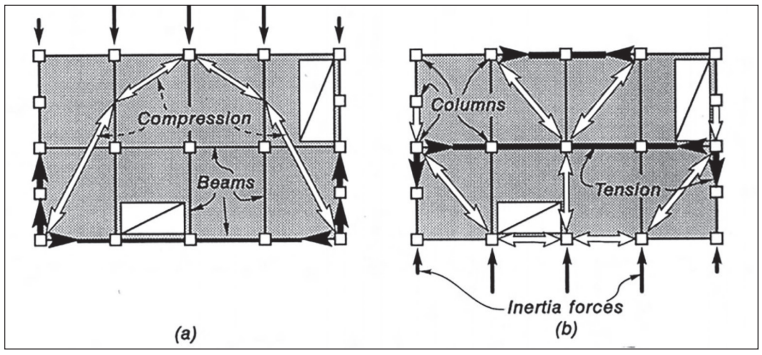

Figure 1: Strut-and-tie load-paths, using diagonal compression fields, for different directions of seismic forces (Paulay 1996)

PAPER CLASS & TYPE: GENERAL REFEREED

1 *University of Canterbury*
2 *University of Auckland*
3 *Holmes Consulting LP*
4 *Compusoft Engineering*
5 *BRANZ*

(a) Significant floor perimeter cracking following the 2011 Christchurch earthquakes (Kam et al. 2011)

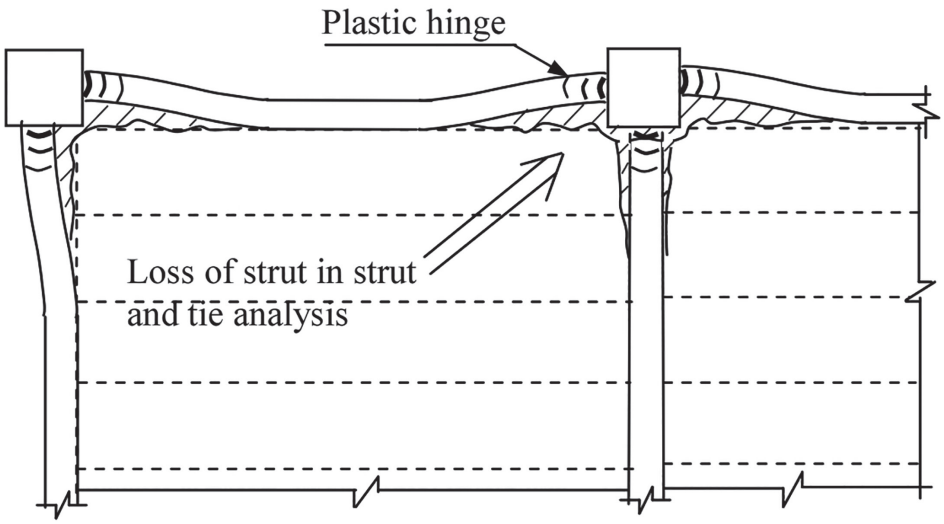

(b) Loss of strut landing points due to significant perimeter cracking (Fenwick et al2010)

Figure 2: Examples of significant floor perimeter cracking and loss of compression strut load paths

Evidence of possible deficiencies with current diaphragm design assumptions for buildings with reinforced concrete frame structures with precast concrete floors was observed in the aftermath of the 2011 Christchurch earthquake. Floors were found with large cracks and openings around their perimeter where they connect to supporting beam and column elements as shown in Figure 2a. This confirmed previous concerns, for example as shown in Figure 2b.

The extensive perimeter floor cracking seen in concrete frame buildings with precast floors is primarily due to beam elongation in the frame. This creates deformation incompatibility between the frame and floor, leading to cracking at weak sections, which tends to be at the interface between the beam and floor. In addition, cracks were observed between individual precast flooring units, providing evidence of diaphragm degradation out in the floor span. Across these cracks it was commonly observed that the floor reinforcing mesh had ruptured, leading to the loss of the tension tie component of the diaphragm load path. Examples of this form of diaphragm damage are displayed in Figure 3.

Figure 3: Cracking between individual precast concrete flooring units and mesh rupture observed following the 2011 Christchurch earthquakes (Henry and Ingham 2012)

These are some of the most recent findings that support concerns that the assumptions justifying the use of the strut and-tie method could be at least partially invalid. This is because the compression strut portion of the load-path cannot cross an air gap (in other words, it is impossible to push on air) and loss of tension ties through mesh rupture also eliminates the viability of the designed load-path.

This research seeks to experimentally investigate diaphragm load-paths throughout different stages of earthquake-induced damage. Based on previous research and post-earthquake observations it is assumed that the designed strut-and-tie load-path for floor diaphragms degrades and (at least partially) fails under sufficient earthquake loading. Leading from this initial assumption, the following questions arise:

- How does the designed load-path degrade with respect to drift demand?
- What is the alternative load-path that develops as the designed load-path degrades?
- What is the residual load sharing capacity of the degraded diaphragm load-path relative to the stiff idealised load-path?

The main useful outcome made clear from previous literature was the necessity of creating a full-scale experimental rig for the floor that included the structural frame of a reinforced concrete building. This was due to multiple observations that the main driver for the development of perimeter cracking is beam elongation in the frame. It would not be possible to create a representative model of diaphragm degradation without realistic frame inelastic response driving the floor damage.

The challenge encountered after these starting decisions was in finding how to load a diaphragm frame specimen in a way that could form a residual diaphragm load path while being representative of a real structure. Previous experimental studies related to earthquake performance of precast flooring units in frame specimens have captured degradation of the floor but did not capture the development of a residual load-path.

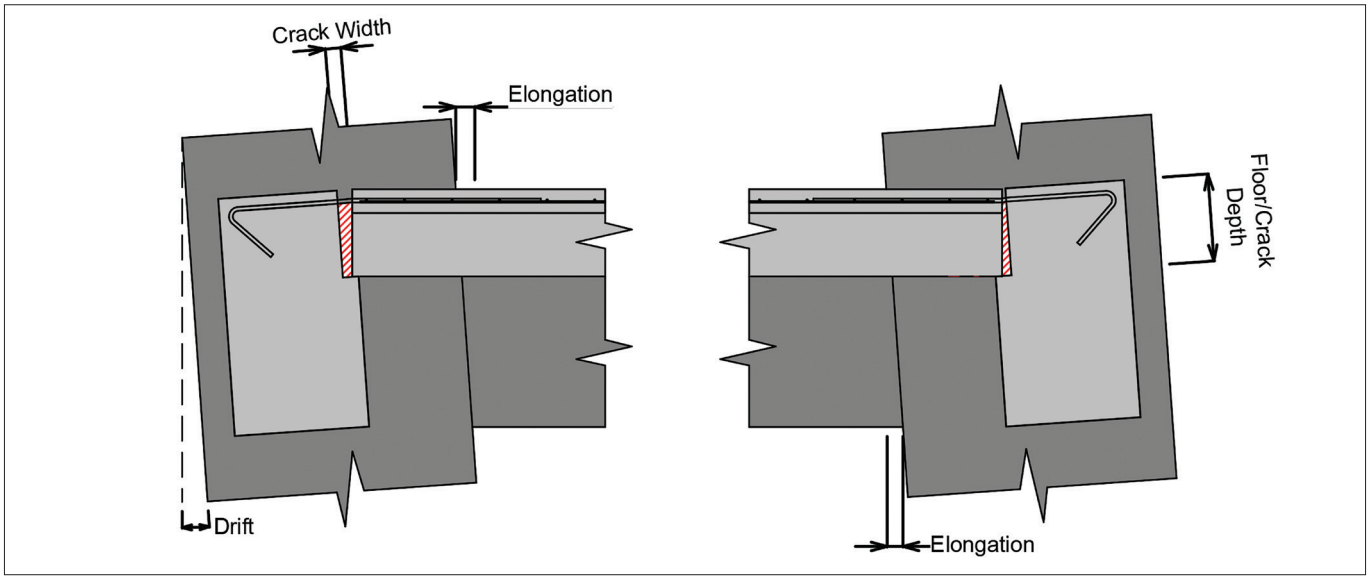

Figure 4: Loss of diaphragm load-path under uni-directional loading

The reason degradation and development of floor load-paths has not been captured in previous literature is because it was not the purpose of previous testing to try and capture these effects. Design of a test that could capture these effects required two core assumptions to be made at the planning phase.

The first of these assumptions is that realistic diaphragm degradation and formation of a residual load path can only develop under simultaneous bi-directional loading conditions with the associated three-dimensional effects. Simple geometry can show that a unidirectional push in either of a frame's primary axes would not lead to suitable binding for load transfer in a floor with wide cracks around the entire perimeter, as shown by the red hatched areas in Figure 4. Additionally, the damage state of the corner of a floor plate would not be realistic under unidirectional loading and this is the most likely zone for a residual load path to form.

As a simple example using rough geometry, for a 275 mm total floor depth (200 mm hollowcore + 75 mm topping) at 3% drift it would require a crack width of approximately 275 mm * 0.03 = 8.25 mm at the beam to floor interface to prevent the possibility of any binding between the floor and frame. Beam elongation for a single plastic hinge can reach to approximately 30 mm, therefore forcing a crack width well above what is required to remove the load-path even under extreme drift demands.

This illuminates the need for simultaneous bidirectional loading to engage a residual diaphragm load-path (or at least "set the stage" for one to develop through the imposed damage state). This is likely a major cause for the lack of available literature on this topic because most pseudo-static earthquake structural experimental studies focus on unidirectional pushes to simplify the results. However real earthquakes do not take into consideration the cardinal directions so simultaneous bidirectional loading is highly appropriate for capturing true diaphragm behaviour.

The second assumption is that the frame does not maintain its shape as the diaphragm degrades, but instead warps in plan. As perimeter cracks become very wide it is likely that simultaneous bidirectional loading would not cause binding of the diaphragm and load transfer between frame elements. However, at this stage of damage the frames would not be linked and therefore would be deforming independently of one another. This would create torsional and warping deformation of the entire structure in plan. Evidence of this kind of structural behaviour was provided in recent shake table testing in Taiwan (Suzuki et al. 2020). If the surrounding frame elements of the floor were to warp into a rhomboidal shape in plan, this could create an intermittent strut from the floor wedging across the diagonals between columns of the warped frame as displayed in Figure 5.

In other words, if the frame undergoes shear deformation in plan, this could wedge the floor and instate a residual load transfer mechanism to link the frames. For pseudo-static testing this would require manually enforcing the shear deformation in plan by moving one frame with hydraulic actuators while keeping the other fixed in the manner shown in Figure 5.

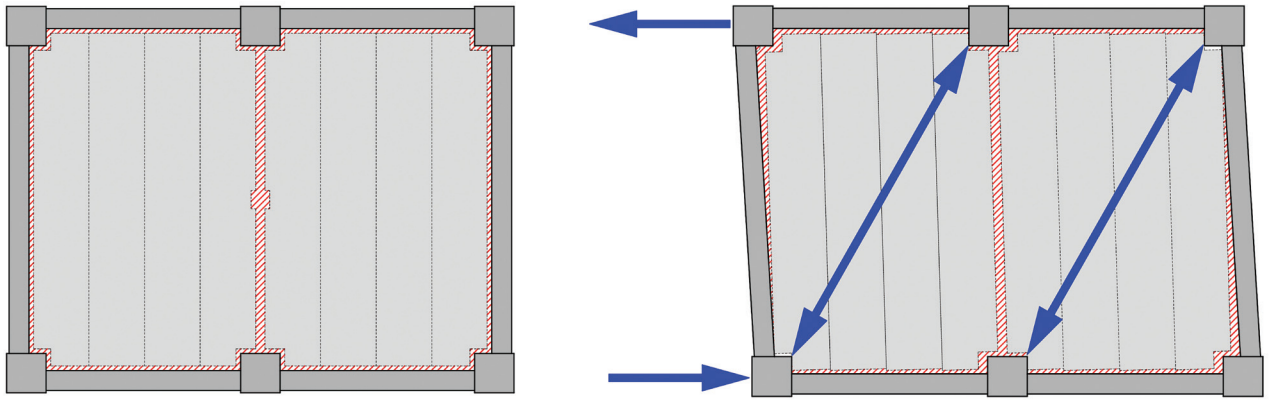

(a) Damaged diaphragm with no viable strut-and-tie load path at perimeter

(b) Shear deformation in plan creating the proposed residual load-path

Figure 5: Proposed residual diaphragm load path – shear deformation in plan creating the "picture frame effect"

This has not been attempted in previous experimental studies on realistically damaged floor specimens, which means it presents a research gap that will be covered by this report. The proposed diaphragm shear distortion residual load path has been compared to a picture sitting within a rectangular frame that is too large for it, meaning it is free to jostle within the frame until it either twists diagonally or the frame warps diagonally into a rhomboid. For simplicity, the effect will commonly be referred to as the "picture-frame effect".

Part I of this journal series explains the design and rationale of the full-scale super-assembly experiment for capturing residual floor diaphragm load-paths and explores the observations made during testing. Analysis of instrument data from the test can be found in Part II (Parr et al. 2022). Further detailed discussion of the experimental layout and loading justification can be found in the thesis (Parr 2022).

2 SPECIMEN DETAILS AND LOADING

As detailed in a companion paper (Büker et al. 2022) the two super-assembly experiments conducted at the University of Canterbury (UFC) during 2020 and 2021 (Fig 8) were designed to provide realistic deformation incompatibility demands under lateral loading into a hollow core floor system via a support frame based on a subsection of a typical ductile reinforced concrete moment frame building. The two experiments used the same frame and hollow-core layout shown in Figure 6.

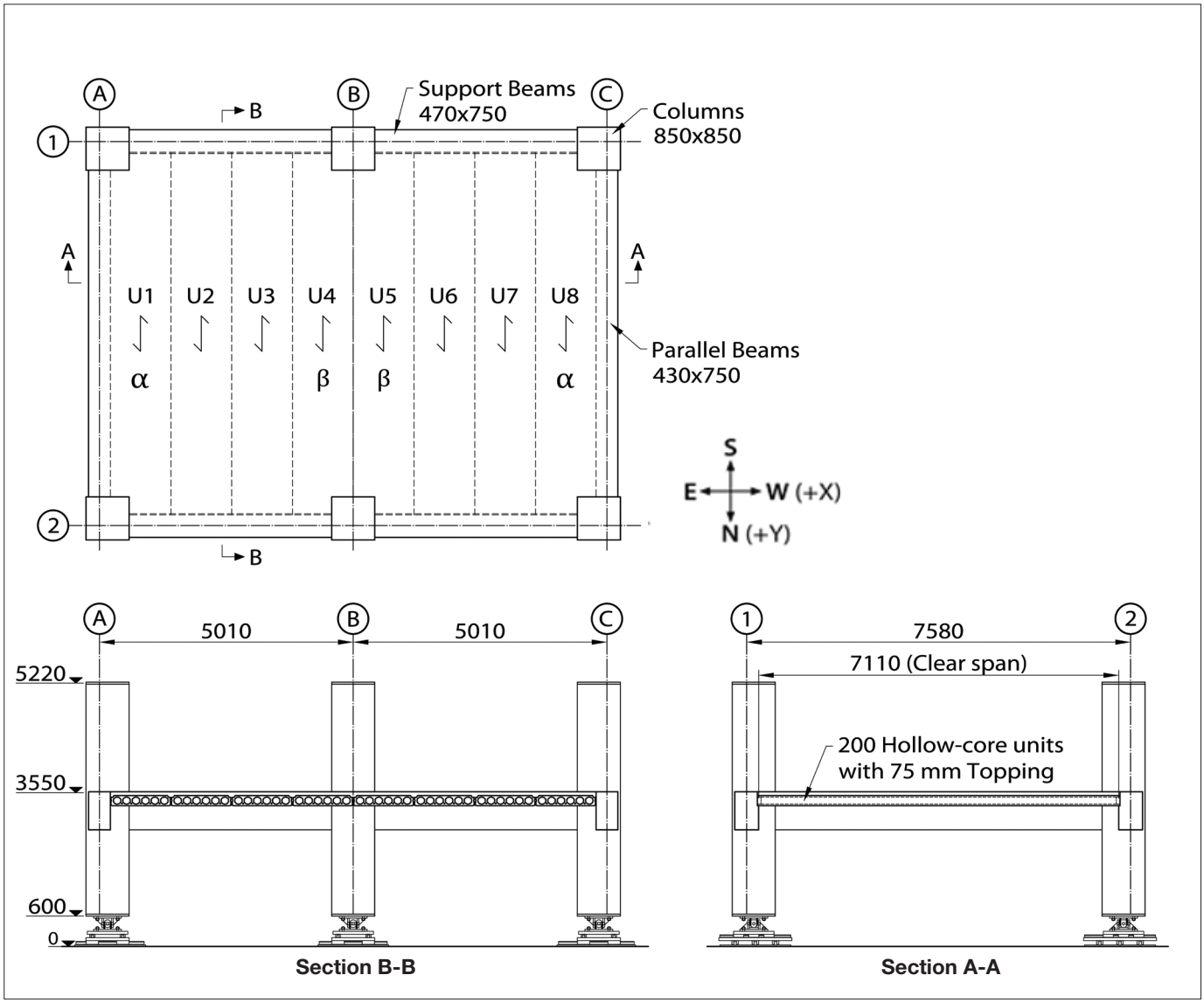

Figure 6: 2020 UC super-assembly experiment frame layout and nominal dimensions (Büker et al. 2022)

When referring to columns or beams their location on the gridlines will be used. For example the south-eastern column would be referred to as column A1 and the beam spanning between column A1 and column B1 would be referred to as beam A1B1.

Hollow-core units in different positions within the floor system are commonly referred to by different names. The units at the end of the floorplate seated on plastic hinge zones of supporting beams next to longitudinal beams are referred to as alpha units (units 1 and 8 in the 2020 UC super-assembly experiment). This is because they have historically been the units of primary concern due to deformation incompatibility with the surrounding frame elements increasing likelihood of catastrophic failure. Interior units seated on beam plastic hinges are referred to as beta units (units 4 and 5 in the 2020 UC super-assembly experiment). This is because they are the units of secondary concern with considerable deformation incompatibility demands with the surrounding frame but were not focussed on as heavily in early research. In this paper units not seated on plastic hinges of the beams (units 2, 3, 6 and 7 in the 2020 UC super-assembly experiment) will be referred to as intra-span units, as they are seated within the span of the supporting beam. Further explanation of terminology related to hollow-core units can be found in a companion paper (Brooke 2022).

The two super-assembly experiments used different floor detailing and loading protocols. The first experiment used a standard starter bar configuration around the entire floor perimeter, cast-in-place tie bars linking the intermediate beams and a linearized circular loading protocol with 1:1 directionality of loading for the standard loading protocol. The first bay of the specimen had no mesh crossing the beam-floor interface. The second bay did have mesh crossing the beam-floor interface to observe the effects of a stronger connection on the hollow-core units, which had been retrofitted against negative moment failure. The layout of this experiment is displayed in Figure 7 (a) and will be referred to in this report as TEST 1.

The second super-assembly experiment used different starter bar configurations at the four support ends of the two bays to encourage targeted local hollow-core failure modes to initiate at the critical end. In the first (eastern) bay, the northern end of the hollow-core units was designed as critical end for failure, targeting loss of seating with a weak mesh-only beam-floor interface. In the second (western) bay, the southern end of the hollow-core units was designed as the critical end for failure, targeting negative and positive moment failures at the end of the starter bars with high strength beam-floor continuity reinforcement. The targeted critical failure ends of each bay were installed on the diagonals opposite each other to minimise interaction of failure modes that could affect results. Additionally, D12 “stitching” bars were installed linking the two beta units (unit 4 and unit 5) to strengthen the connection after results from the TEST 1 experiment determined that this was a critical weak point for both the gravity carrying and diaphragm functions of the floor. The layout of this experiment is displayed in Figure 7 (b) and will be referred to in this report as TEST 2.

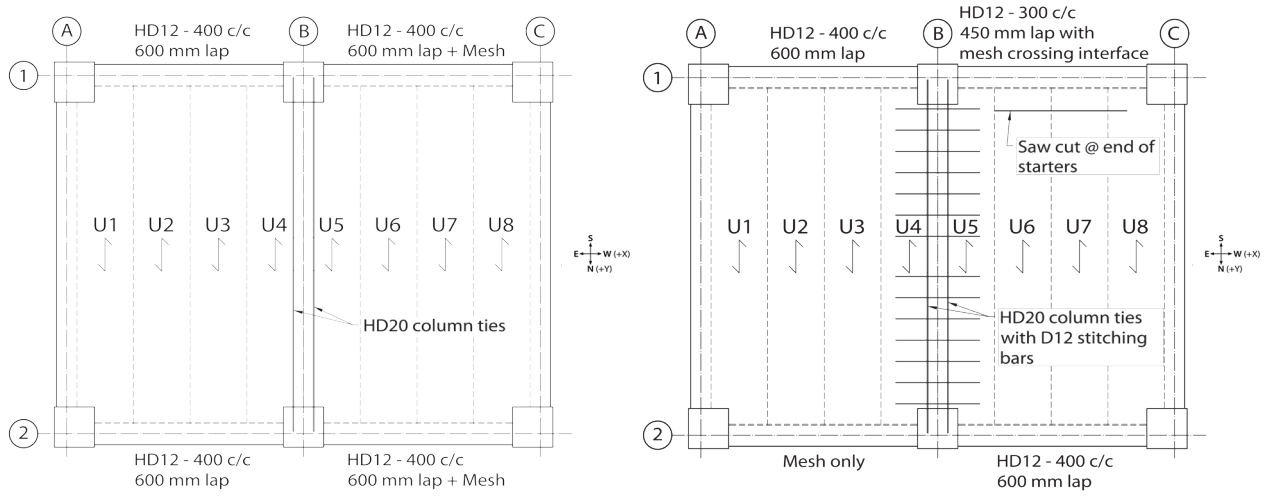

(a) TEST 1 Continuity Reinforcement

(b) TEST 2 Continuity Reinforcement

Figure 7: Floor continuity reinforcement arrangements for TEST 1 and TEST 2 (Büker et al. 2022)

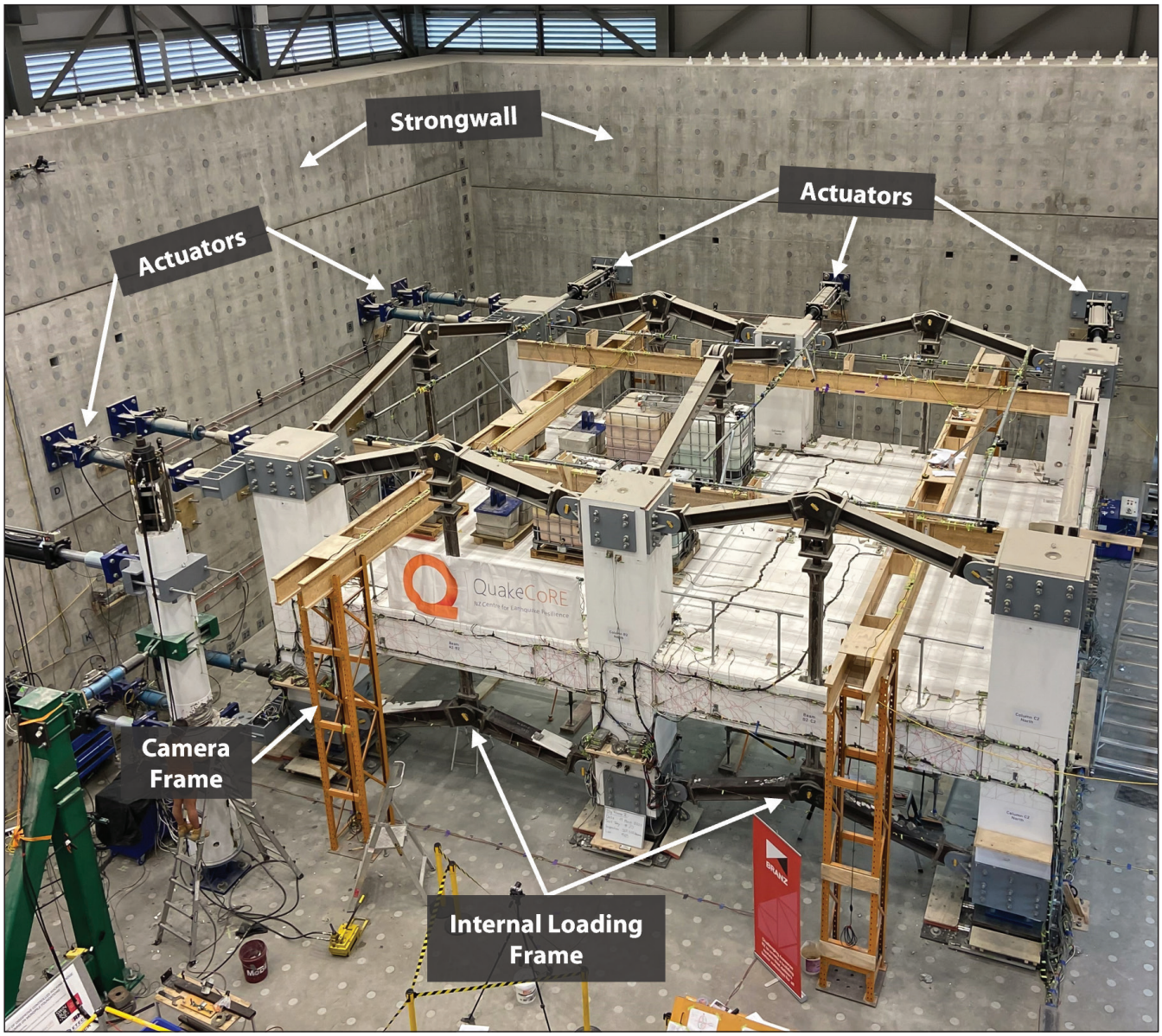

Figure 8: Experimental layout of the 2020 University of Canterbury super-assembly experiments (Büker et al. 2022)

Displacement demands were applied to the specimen using an arrangement of fourteen hydraulic actuators pushing and pulling from a strong-wall as shown in Figure 8.

Internal loading frames consisting of arrow-frames and bi-directional frictionless sliders were used to enforce realistic demands between individual columns. The objective was to keep the columns parallel during loading while avoiding restriction or promotion of beam-elongation. This was done to ensure the forces and deformation incompatibility applied to the floor was representative of a real structure subjected to lateral loading.

The control software for the actuators was programmed to allow the structure to grow from beam-elongation outward from the origin at column A1 depicted in Figure 9. The concept of how the arrow-frame and bi-directional sliders also facilitated this structural growth is shown in Figure 10. Further details on the design philosophy of the experiment can be found in the thesis (Parr 2022).

The beam-column casting interfaces of TEST 1 and TEST 2 were different. The bottom half of the longitudinal beams in TEST 1 were cast with the pre-cast columns, meaning there was no cold-joint. The top half of the longitudinal

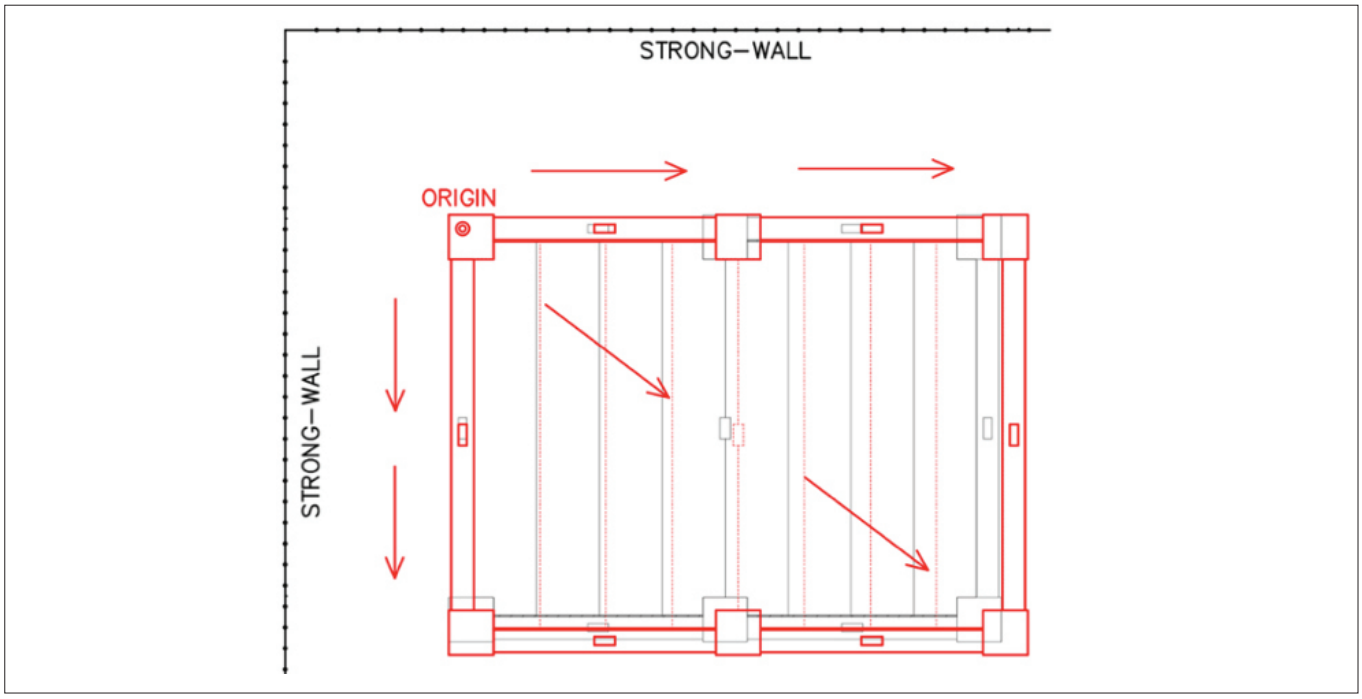

Figure 9: Specimen growth from the origin at column A1 due to beam elongation

beams were cast in-situ and had a smooth casting surface against the pre-cast column interface. The support beams of TEST 1 were cast in-situ and had an array of slightly roughened and smooth casting interfaces with the pre-cast columns.

After observations in TEST 1 of beams losing torsional stiffness (as discussed in Section 3), all beams in TEST 2 were cast in situ against purposely roughened column interface surfaces to provide better interlock across the cold joint.

TEST 1 and TEST 2 also used different standard loading protocols. TEST 1 used a linearised circular loading protocol with directionality 1:1 to enforce the widest range of possible deformations on the specimen and floor as shown in Figure 11 (c). This was considered as the upper bound of directionality expected from an earthquake. After the findings detailed in Section 3 and Part II (Parr et al. 2022) related to TEST 1, it was decided that TEST 2 would have a more targeted directionality typical of a pulse or near-fault earthquake shaking.

This led to the use of a 2:1 directionality linearised oval protocol as shown in Figure 11 (d). This was considered as the lower bound of likely realistic earthquake directionalities based on research conducted by Nievas and Sullivan (2017). This meant TEST 1 and TEST 2 would provide an upper and lower bound of simultaneous bi-directional actions imparted into a floor system respectively.

TEST 1 began with an approximation of the 2016 Kaikoura Earthquake drift cycles for the prototype Wellington building the specimen was based on to allow comparisons to damage modes observed in real buildings. A standard circular loading protocol of increasing drift demands was then applied as shown in Figure 11 (a). TEST 2 started with an approximation of the 1994 Northridge Earthquake to simulate a pulse style loading followed by a standard oval loading protocol of increasing drift demands as displayed in Figure 11 (d).

At selected locations within the TEST 1 and TEST 2 loading protocols, the loading was switched to a rhomboid loading protocol to enforce plan shear distortion into the floor diaphragm and assess the diaphragm load paths. The locations where the standard loading protocols (SLP's) were stopped for rhomboid loading in TEST 1 and TEST 2 are displayed in Figure 11 (a) and (b).

The locations for stopping the standard loading protocol to perform a rhomboid loading protocol were chosen based on the desire to compare the stiffness and load path changes from a relatively undamaged floor diaphragm to

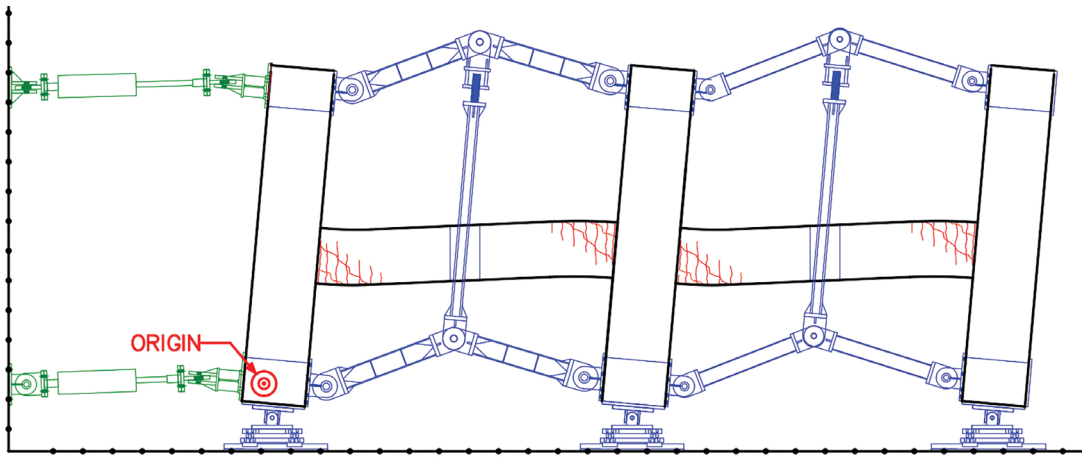

(a) Super-assembly specimen when subjected to positive east-west drift demands

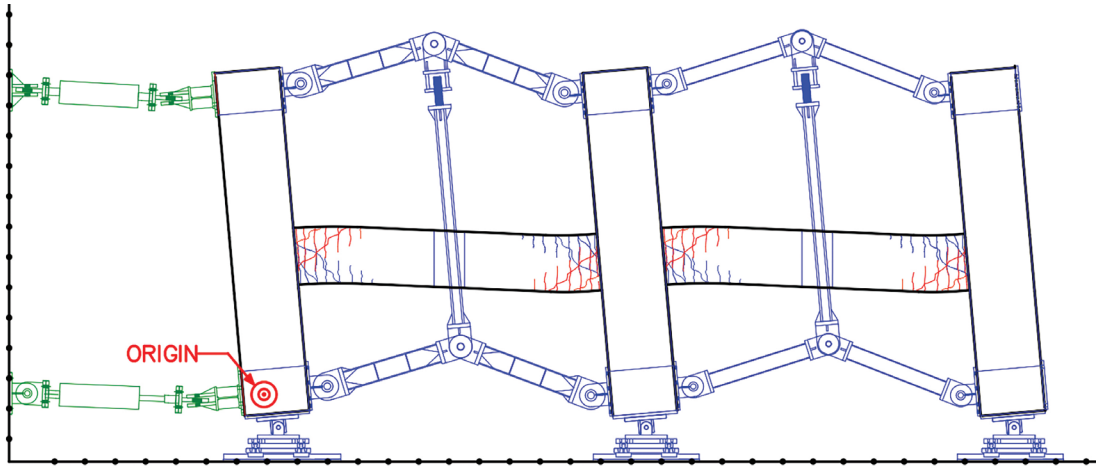

(b) Super-assembly specimen when subjected to negative east-west drift demands

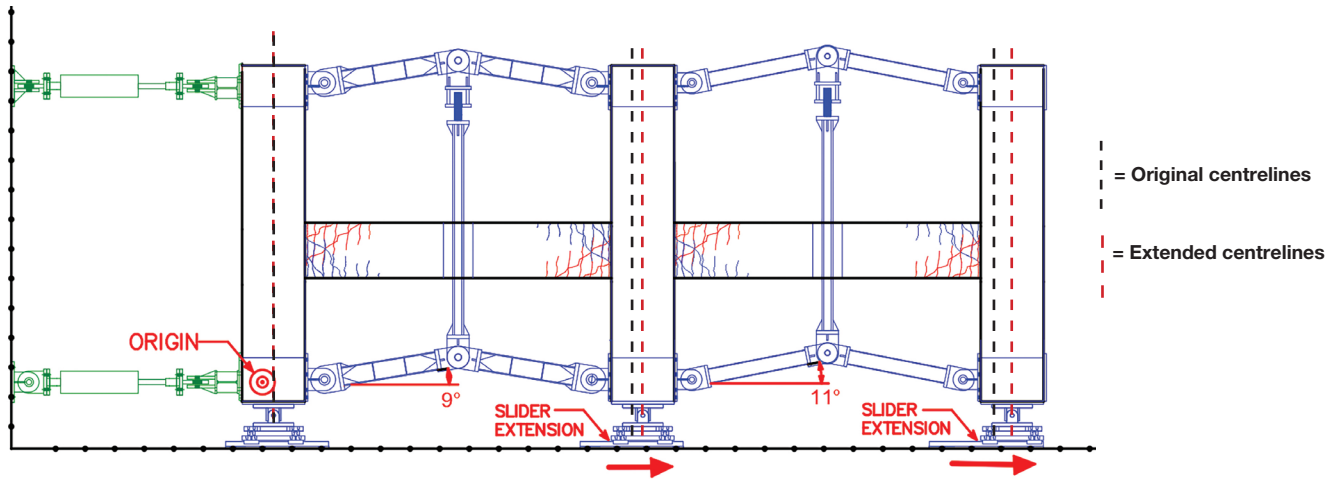

(c) Super-assembly specimen after growth due to beam elongation following reverse cyclic demands

Figure 10: Loading frame system allowing for specimen growth without restraining or promoting beam elongation in the 2020 UC super assembly experiments

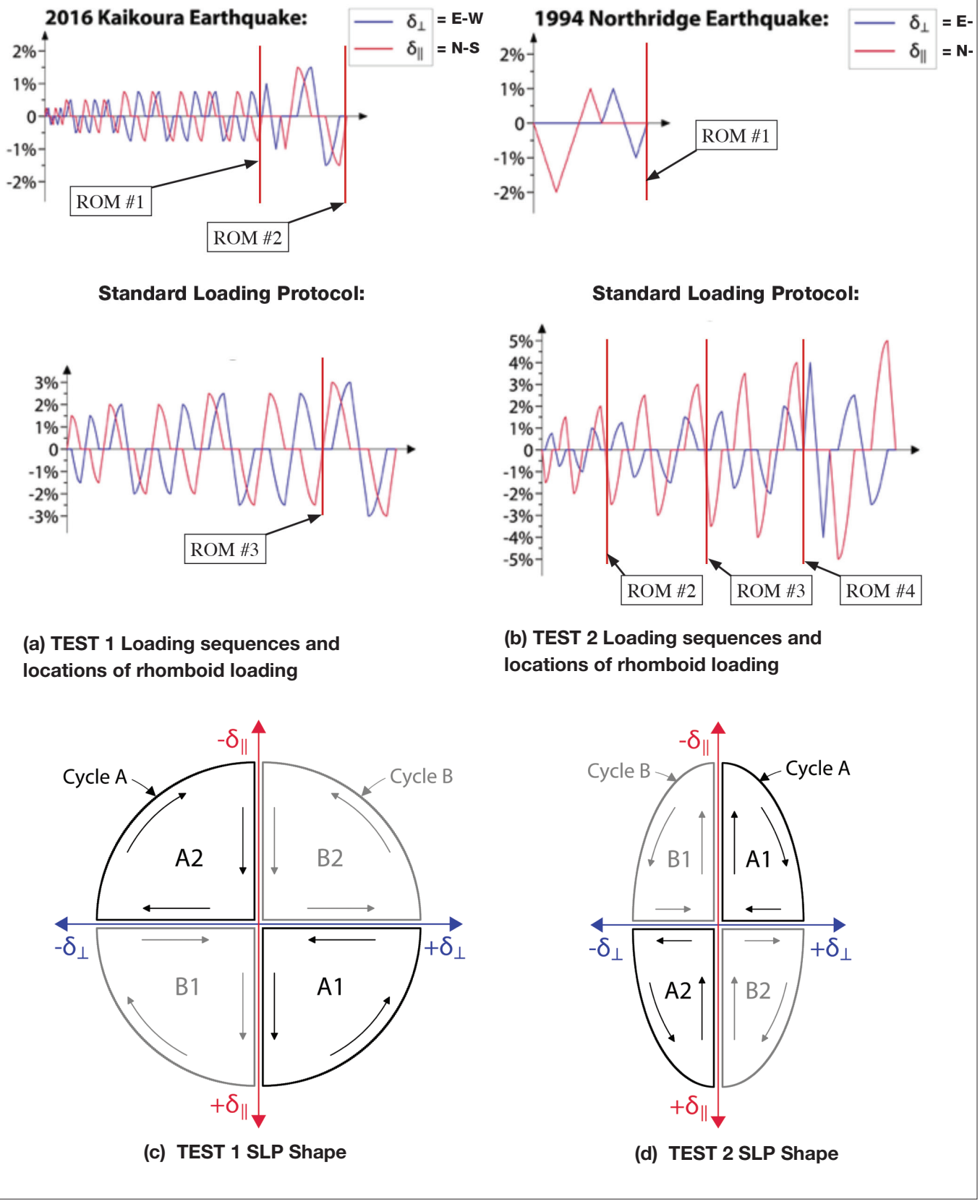

Figure 11: Standard loading protocols and locations of rhomboid loading protocols for the TEST 1 and TEST 2 experiments (Büker et al. 2022)

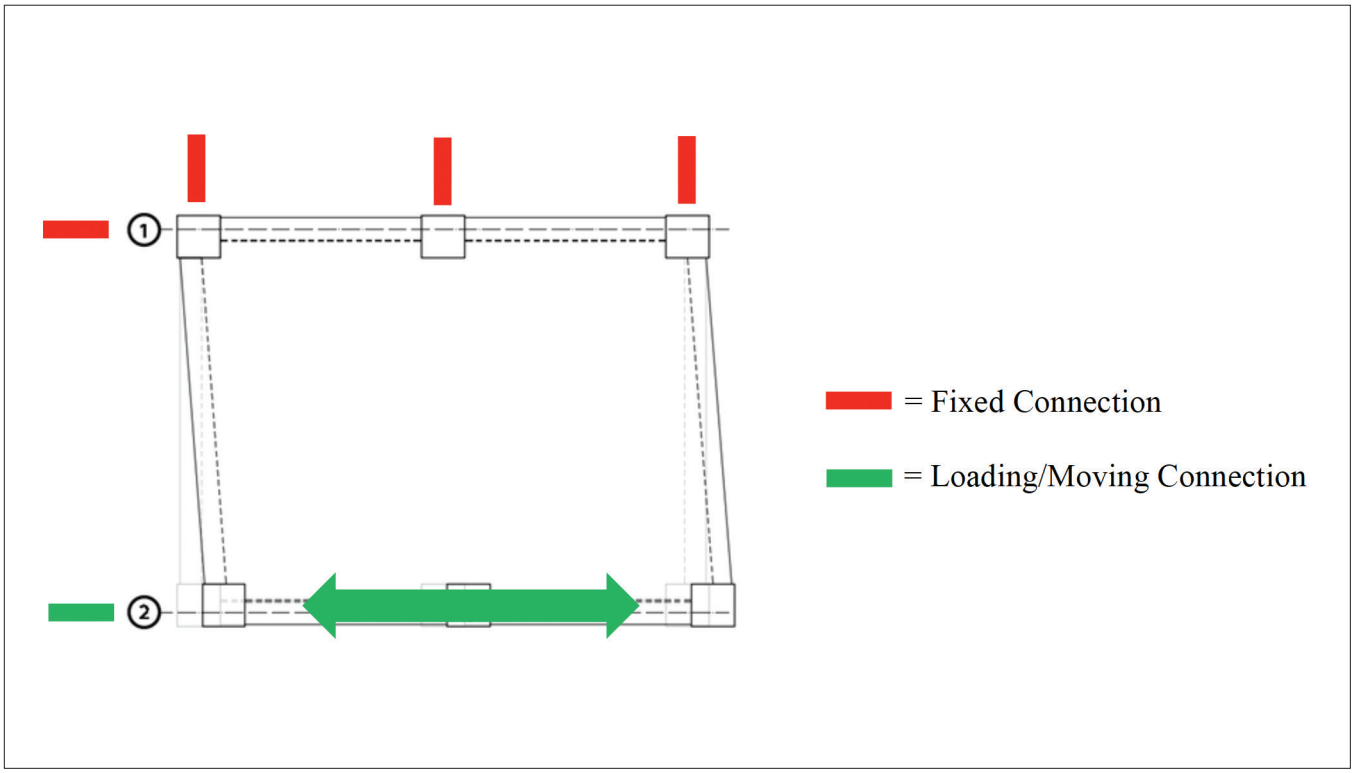

Figure 12: Fixity and loading of the specimen during rhomboid loading (positive shear distortion shown)

the same diaphragm when it was partially damaged and heavily damaged. This would allow for observation of the degradation of the designed load-path and formation of true residual load-paths.

Each rhomboid loading protocol was undertaken once the specimen was brought back to the closest approximation of residual drift that could be achieved after the previous standard loading cycle. The fixities of the loading system for the rhomboid loading protocol are displayed in Figure 12.

As shown in Figure 12 the south frame (frame 1) was held stationary by all actuators attached to columns A1, B1 and C1. The north frame (frame 2) was driven with positive and negative displacements in the east-west direction via the double actuator configuration attached to column A2 to enforce shear distortion on the specimen floorplate in plan. No drift was applied during the rhomboid loading protocols as it was desired to isolate the effects of shear distortion for determining diaphragm load-paths.

The magnitude of each rhomboid loading protocol was different depending on the level of damage the specimen had sustained in previous standard linearised circular loading cycles. Early rhomboid loading protocols within each test (TEST 1 and TEST 2) were force controlled and had small maximum displacements, with each subsequent rhomboid protocol within a test increasing the displacement demand. This was done to avoid prematurely damaging the specimen before it had softened from the standard loading protocol. Higher deformation was imposed for the final TEST 2 rhomboid compared to TEST 1 as it was the specimen's end-of-life with no further refurbishment planned.

Table 1: TEST 1 and TEST 2 Rhomboid applied displacement and shear distortion demands

Rhomboid #	+- Plan Shear Distortion, γ (%)				Targeted state of the diaphragm for testing
	Test 1		Test 2		
	± Shear Distortion, γ (%)	± Force (kN)	± Shear Distortion, γ (%)	± Force (kN)	
1	0.01	250	0.005	250	No/low damage to designed load-paths
2	0.05	500	0.02	500	Intermediate damage to design load-paths
3	0.11	450	0.06	600	High damage to designed load-paths
4	n/a	n/a	0.25	700	Extreme damage to designed load paths

3 EXPERIMENTAL OBSERVATIONS

The critical observations relating to the diaphragm behaviour for both TEST 1 and TEST 2 are described in this section.

3.1 DIAPHRAGM DAMAGE OBSERVED FROM STANDARD LOADING PROTOCOLS

By 0.25% drift, the damage modes and crack patterns observed in the TEST 1 and TEST 2 diaphragms had diverged significantly. This was due to the difference in directionality of the standard loading protocols as well as the beta-beta unit stitching retrofit installed in the TEST 2 specimen.

The TEST 1 specimen developed a full-length split between the beta-beta unit interface at 0.25% drift. Further damage concentrated at this split in later cycles with mesh rupture along the interface occurring in the first arc loading at 1.5% drift. From this point on, the two bays of the specimen acted as separate floor plates. There were early signs of cracks developing in the floorplate at the ends of starter bars up to approximately 1.5% drift, but in future cycles, these cracks were observed closing compared to previous cycles. The closing up of inner floor cracks coincided with observations that the beams were beginning to rotate torsionally into the structure. Development of additional significant cracking relevant to diaphragm performance from this stage was limited to the topping located near plastic hinge zones of the beams, particularly in the corners of the overall floorplate where seating of the alpha units was located. An example of significant beam torsion observed at the end of the TEST 1 test in a support beam is displayed in Figure 13. Note that the black lines drawn near the bottom corners of the beam aligned with the original location of the beam face.

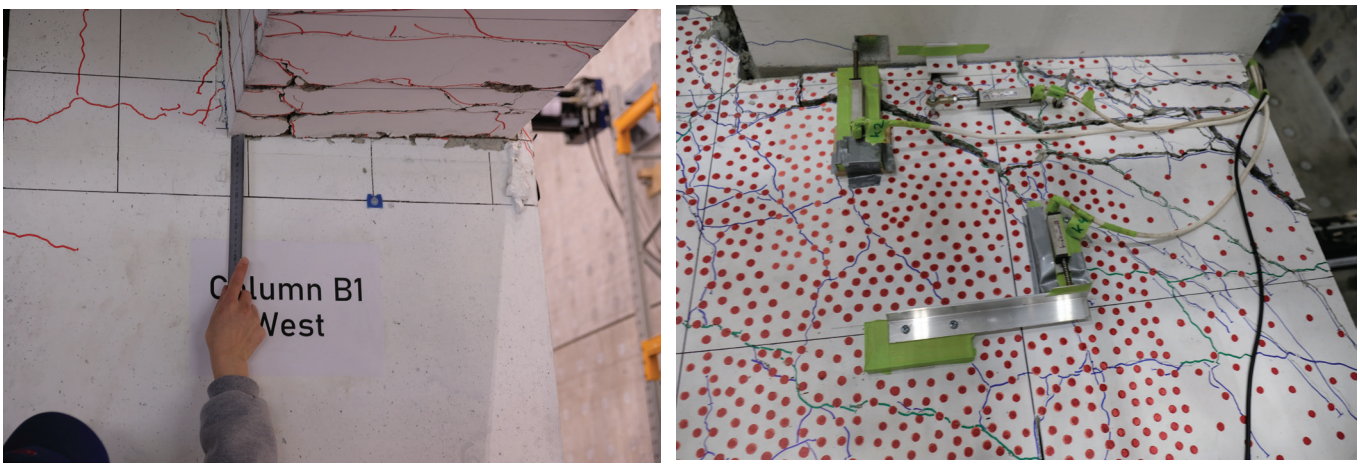

Figure 13: Significant beam torsion visible at the conclusion of the TEST 1

The TEST 2 specimen developed wide cracks at the end of the starter bars on the south end of the floor and at the beam-unit interface on the north end of the floor, with mesh rupture occurring at approximately 1.5% as discussed in (Büker et al. 2022). Cracking occurred between most units, but these cracks were small and distributed compared to the major beta-beta unit crack observed in the TEST 1 test. Other than the improved performance between the beta-beta unit interface, the visible damage in the floor was significantly more severe in TEST 2, with end of starter bar and beam-unit interface cracks with widths of approximately 30-40 mm and 30 mm vertical offset by the end of the test. These extremely wide cracks were useful to compare against those observed in real buildings, where there have been concerns that compression struts could not form across perimeter cracks, destroying the diaphragm load-path.

The crack patterns recorded at the end of TEST 1 and TEST 2 are displayed in Figure 14, depicting the different damage modes observed between them. Hairline cracks and cracks that closed following primary damage modes forming are removed in Figure 15 to allow for easier comparison of the primary damage modes.

Note that the primary floor cracking damage in TEST 1 ran in the north-south direction, the primary example being the split between the two beta units which caused the two bays to act independently from 1.5% drift onwards. Other than this major crack most damage was contained to areas near the beam plastic hinge zones. In TEST 2 the primary floor cracking damage ran in the east-west direction, at the end of the starter bars on the south end and at the beam-floor interface on the north end. This was due to the stitching bar retrofit strengthening the beta-beta unit interface and the directionality of loading being more critical in the north-south direction compared to TEST 1.

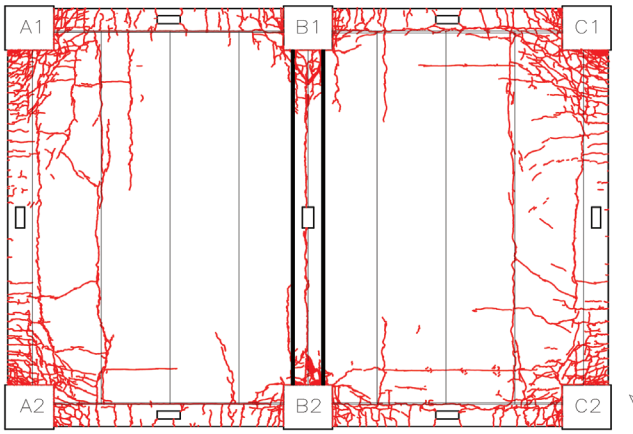

(a) TEST 1 Topping crack map after 3.0% drift

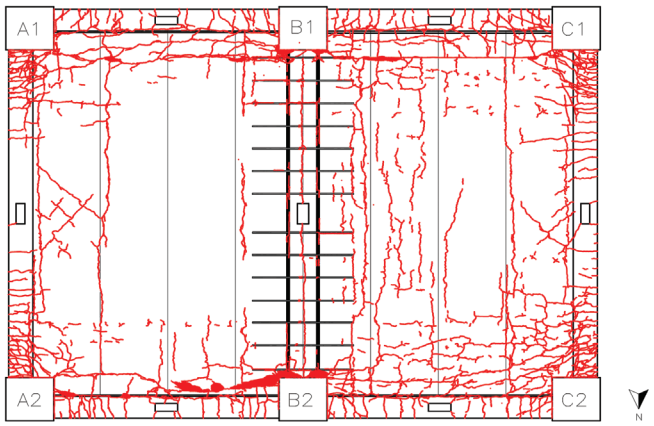

(b) TEST 2 Topping crack map after 5.0% drift

Figure 14: Topping crack maps for TEST 1 and TEST 2 at conclusion of experiments

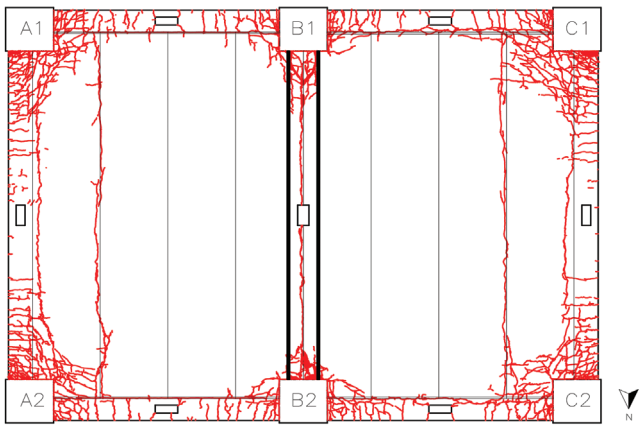

(a) TEST 1 Topping crack map showing only wide/important cracks demonstrating the observed load-paths

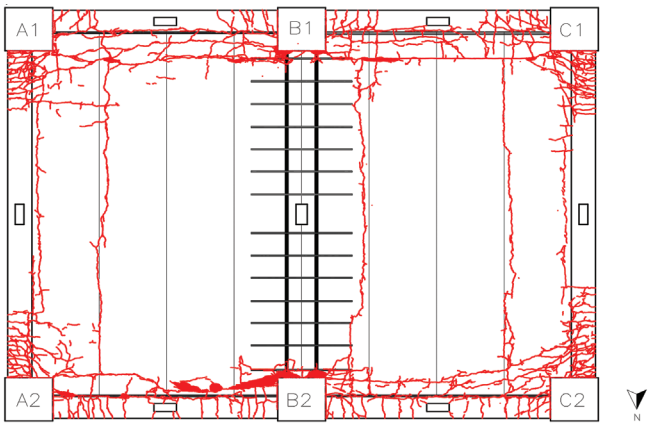

(b) TEST 2 Topping crack map showing only wide/important cracks demonstrating the observed load-paths

Figure 15: Topping crack maps for TEST 1 and TEST 2 at conclusion of tests with only critical wide cracks impacting load-paths visible

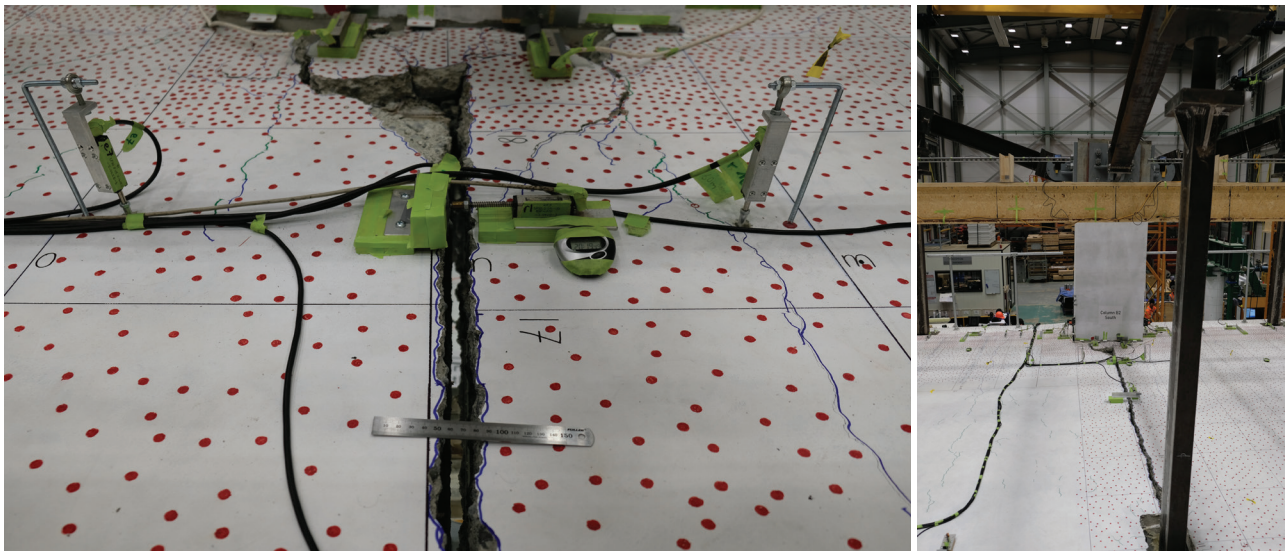

(a) TEST 1 Beta-beta unit interface crack following 3.0% drift demands

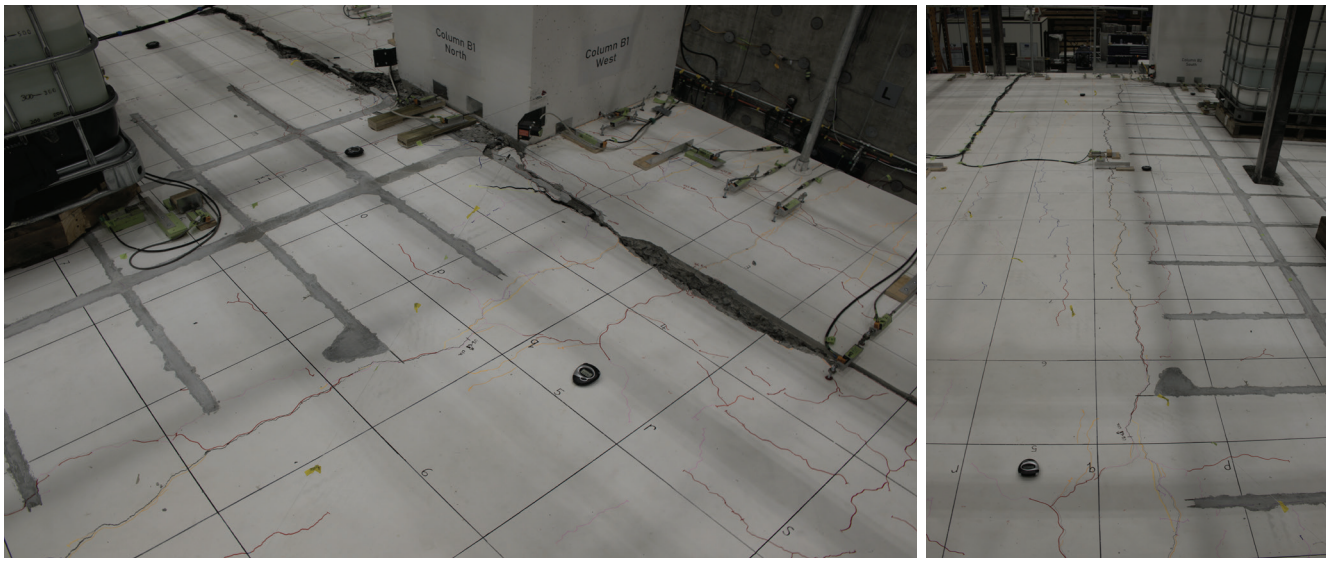

(b) TEST 2 Unit 5 – Unit 6 crack (only developed under large shear distortion demands after 4.0% drift)

Figure 16: Comparison of inter-unit cracking near the beta units between the TEST 1 and TEST 2 experiments

A comparison between TEST 1 and TEST 2 of the beta-beta unit interfaces near the end of both tests is displayed in Figure 16.

The stitching bars succeeded in preventing significant cracking developing between the two beta units, with a maximum beta-beta unit crack width recorded of approximately 0.2 mm. Instead multiple smaller cracks developed along and between units. As there was no mesh rupture or wide cracks this meant diaphragm actions could develop across both bays. This was the case until the 4th rhomboid when significant shear distortion in the positive direction (at a γ value between 0.23% and 0.25%) caused a large split to occur between unit 5 and unit 6 near the end of the stitching bar retrofit.

A comparison between the TEST 1 and TEST 2 experiments of cracking at the end of the starter bars at the south end of the floor near the end of both tests is displayed in Figure 17.

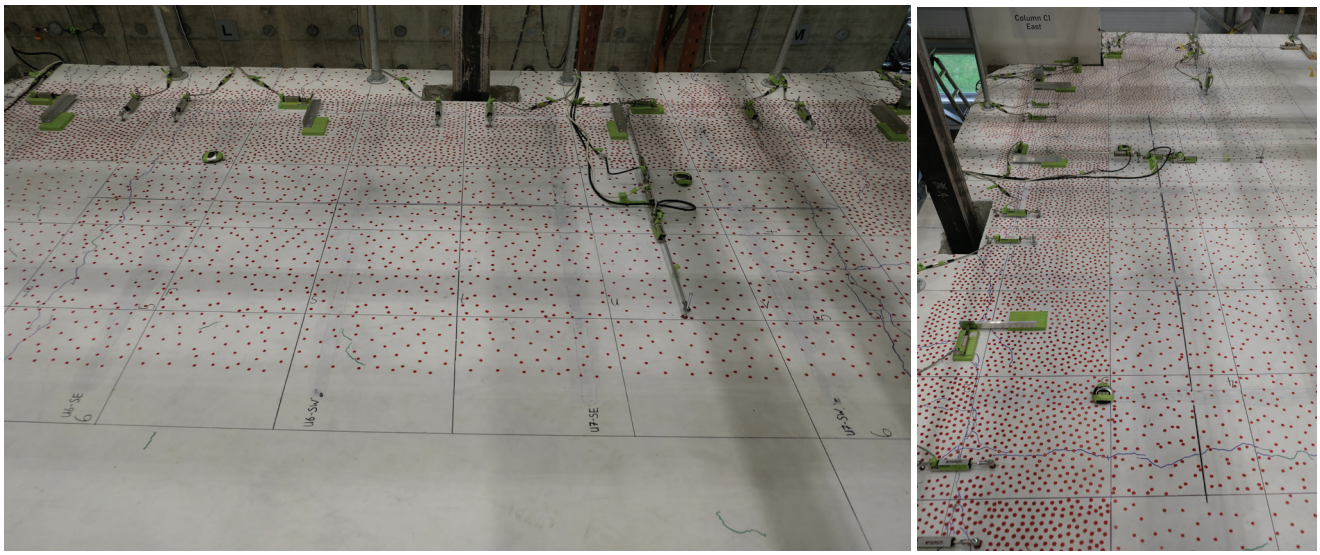

(a) TEST 1 End of starter bar cracks following 3.0% drift demand

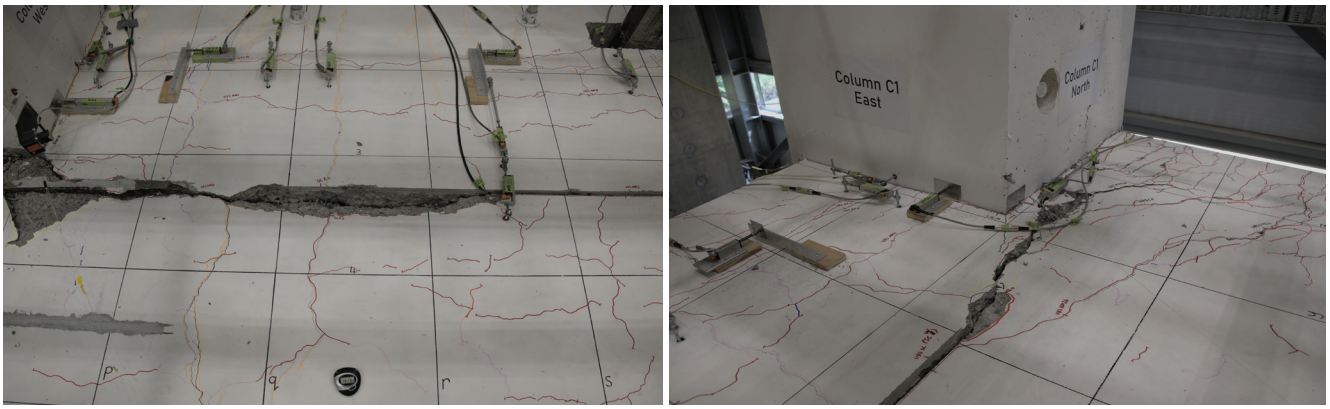

(a) TEST 2 End of starter bar cracks following 4.0% drift demand

Figure 17: Comparison of cracking at the end of starter bars on the south end of the floor between the TEST 1 and TEST 2 experiments

The TEST 2 specimen sustained much greater damage at the end of the starter bars compared to the TEST 1 specimen. This was primarily due to the change in directionality of loading protocols with less beam torsional softening observed in TEST 2 due to the reduction of simultaneous demands. An additional factor altering the strength hierarchy of the beam torsional capacity vs floor strength between the two tests was the additional roughening of the cold joint between the column concrete element and beam concrete elements in TEST 2 as described in Section 2. These factors meant the beams remained stiff enough to impart large deformation incompatibility demands into the floor units, leading to significant early cracking.

By approximately 1%-1.5% drift in both tests, openings were observed around the entire perimeter of the floor-to-column interfaces, removing any possibility of diaphragm compression struts landing directly into the columns including into the intermediate columns B1 and B2. These openings grew wider with subsequent drift cycles. This means that early in the earthquake record the only remaining diaphragm load path to link the frame elements was through the beams. The only caveat to this general rule was where the tie-bars were anchored into the intermediate columns, though these would not have provided a significant stiff load-path as they were only two D20s acting in compression and dowel action for the purposes of landing compression struts into the columns.

(a) Gaps at column A1 (Alpha unit-column)

(b) Gaps at column B1 (Beta unit-column)

Figure 18: Gaps between the floor and columns at 1% drift in TEST 1

In both experiments significant cracking and spalling of the topping occurred around the tie-bar connections into the column interface. This made the tie-bars visible at higher drift levels, which were clearly plastically deformed by deformation incompatibility between the beta units and columns. The cone shaped spalling failures this caused in the nearby concrete through bond stresses are displayed in Figure 19.

After significant cracking of the topping and hollow-core units in TEST 2 (at >2.5% drift) light could commonly

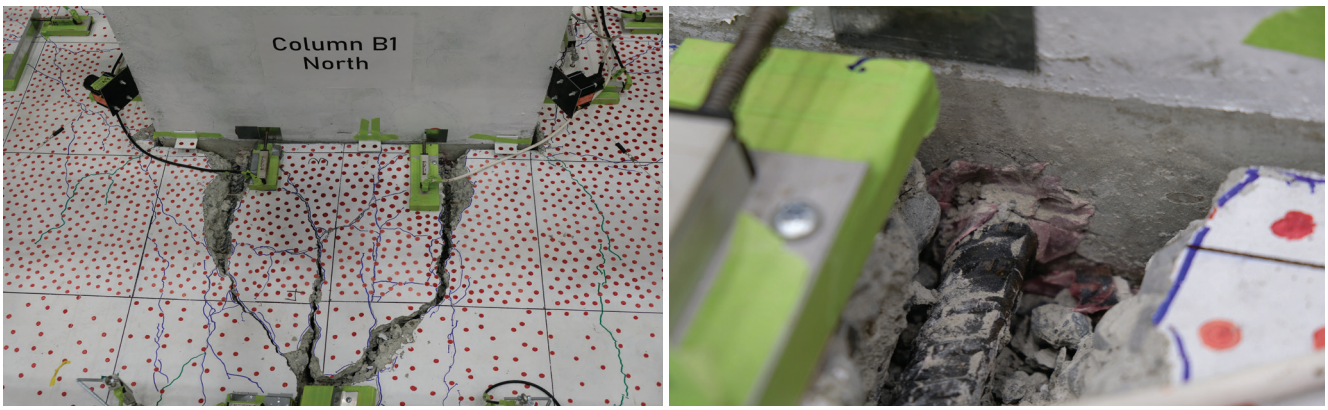

(a) TEST 1 Tie-bar anchorage rubble formation at 3.0% drift

(b) TEST 2 Tie-bar anchorage rubble formation at 4.0% drift

Figure 19: Tie-bar anchorage rubble formation observed in the super-assembly experiments

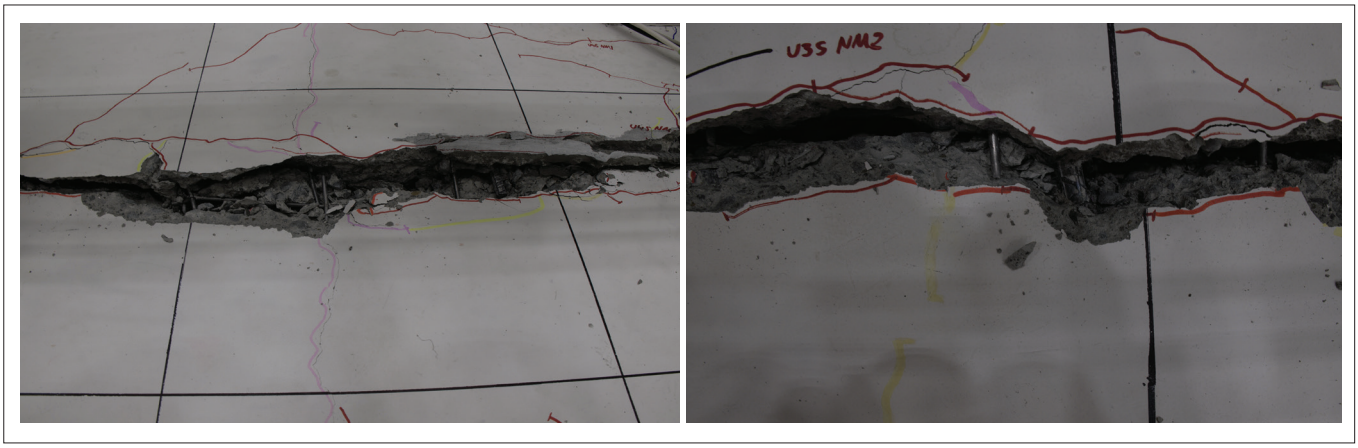

Figure 20: Starter bars and mesh initiating rubble formation within floor cracks

be observed through the wide cracks at the end of the southern starter bars, indicating small gaps where no compression struts could cross. However, these gaps were intermittent with small pieces of rubble falling into the gaps clogging the view through the crack.

The dislodgement of rubble was particularly noticeable near starter bars. The ends of the starter bar would scrape against the other side of the crack, dislodging pieces of aggregate and dropping them into the crack as shown in Figure 20. In these areas it was not possible to see through the crack and it could be reasonably assumed that rubble became lodged, forming small pathways for compression to be transferred across the crack through contact stresses.

While starter bars appeared to be primary initiators of rubble formation it also was also formed in spaces between starter bars, possibly assisted by bond with mesh. Contact stresses under cyclic loading between the two sides of cracks (and with previously formed pieces of aggregate rubble) sheared off protruding pieces of aggregate from the crack face, generating more rubble. The process appeared to be a self-replenishing system creating contact stresses across the crack provided initial rubble was generated to start the process (and a sufficient gravity load-path existed, which was provided in TEST 2 by the cable catch frame system and cantilever seating retrofits described in (Büker et al. 2022)).

The most obvious case of rubble formation providing a contact stress load-path across a crack occurred on the east side of column B2. A large wedge of concrete became detached from the topping and hollow-core at approximately 2.0% drift as shown in Figure 21.

However it was not possible to remove the detached wedge at any stage of the load protocol until approximately 5.0% drift. Between these drift demands the concrete wedge was under compression, with the wedge slowly being pushed up by the formation of rubble on either side.

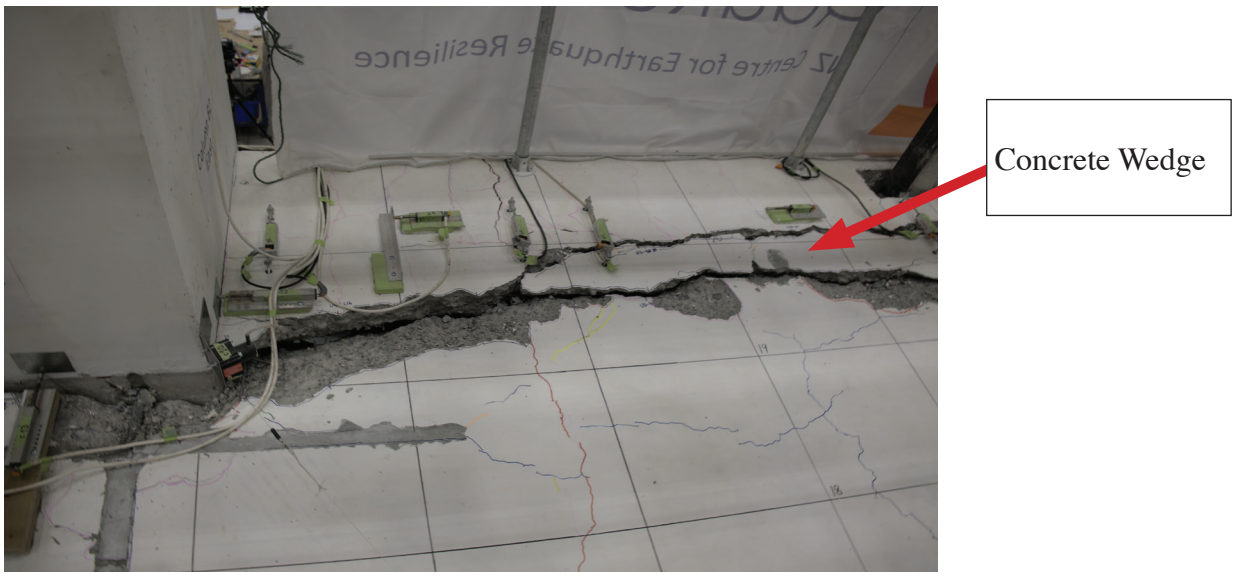

Figure 21: Beam-unit crack interface concrete wedge on east side of column B2 at 4.0% drift

3.2 DIAPHRAGM DAMAGE OBSERVED FROM RHOMBOID LOADING

The three rhomboid loading protocols conducted in TEST 1 did not display any obvious visual signs of damage other than for the third and largest rhomboid loading. This was by design, as it was undesirable to push the specimen to damage inducing deformations in the rhomboids as this could adversely affect the reliability of subsequent results for the hollow-core and future rhomboid results. The obvious impact of standard testing on the diaphragm load-path was the splitting of the two bays causing them to act as individual floorplates. In the third rhomboid a loud crack was heard at a shear distortion of approximately 0.11%. On observation of the topping it was found that a piece of cover concrete on the top of the B2C2 beam western plastic hinge had spalled off the beam and been propelled onto the floor. Another loud crack was heard at a shear distortion of approximately -0.11%. A similar observation was made of cover concrete being disturbed and left loose on the top of the western end of beam B1C1.

These observations provided evidence that the diaphragm compression struts were being transferred to the C1 and C2 columns via the support beam plastic hinges. They also provided evidence that the beam plastic hinges were deforming under the diaphragm loads and were the weak point of the system. The plastic hinges following crushing of the cover concrete are displayed in Figure 22.

The four rhomboid loading protocols conducted in TEST 2 displayed interesting behaviour related to residual compression load-paths across wide cracks. In the 2nd rhomboid, diagonal cracking was observed on the side of a wide crack as shown in Figure 23. This cracking provides evidence of significant local compression across the crack leading to landing of the strut into beam A1B1 towards column B2.

In the 4th rhomboid of the TEST 2 experiment, the diaphragm was pushed to a much greater shear distortion compared to other rhomboids, allowing for significant damage modes to form for observation. The most notable

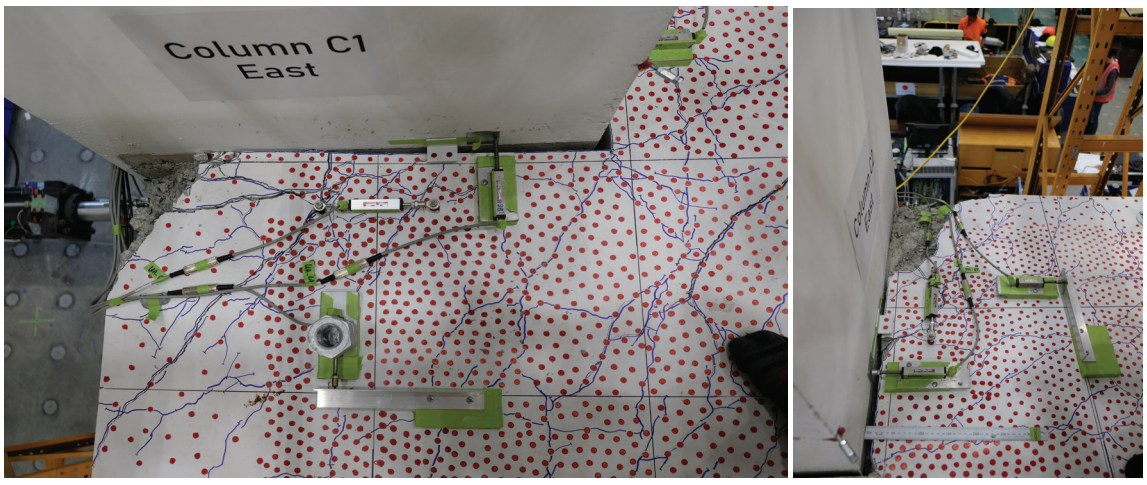

Figure 22: Beam plastic hinge spalling about weak axis from plan shear distortion demands

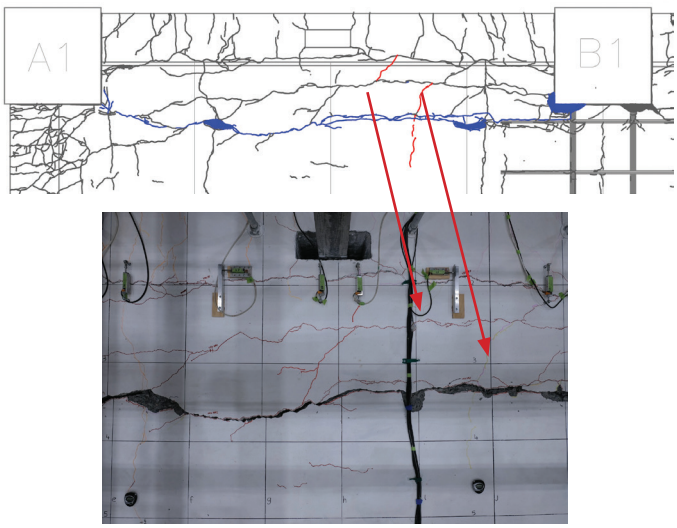

Figure 23: Diagonal cracking displaying local compression strut across wide crack at southern end of units 1-4

Figure 24: Significant split between Unit 5 and Unit 6 that developed in the TEST 2 4th Rhomboid

damage that developed from this loading was mesh rupture and splitting between unit 5 – unit 6 near the end of the stitching bar retrofit as shown in Figure 24.

This rupture occurred at a shear distortion γ in the positive direction between 0.23% and 0.25%. Mesh rupture was observed along approximately 2/3rds of the length from the north end. The crack was much wider at the north end with a width of approximately 7 mm and 4.5 mm vertical offset (with the beta units dropping). At the south end this reduced to approximately 3 mm with no vertical offset. This shows that at the northern end there were significant tensile forces across the crack due to the diaphragm internal strut-and-tie load-path. This is discussed further in Part II (Parr et al. 2022).

Additionally in the 4th rhomboid of TEST 2 a residual load-path was observed landing compression struts directly into the column faces of the intermediate columns (B1 and B2). As shown in Figure 25, as a result of loading in the positive direction, a section of the topping near the eastern tie-bar in column B1 spalled due to crushing failure. Upon observation of the gap between the column and beta unit it was not possible to see through the gap near the tie-bar. This was due to the significant spalling of the topping caused by bond stresses with the deformed tie-bars. The spalled concrete rubble had fallen and wedged between the beta units and interior column face of the intermediate columns. This formed a residual diagonal contact stress compression strut load-path directly from the diaphragm into the column face. Under negative loading similar damage was observed from struts landing into the western tie-bar anchored in column B1. The topping spalling from compression struts landing directly into column B1 is displayed in Figure 25 (b) and (c)

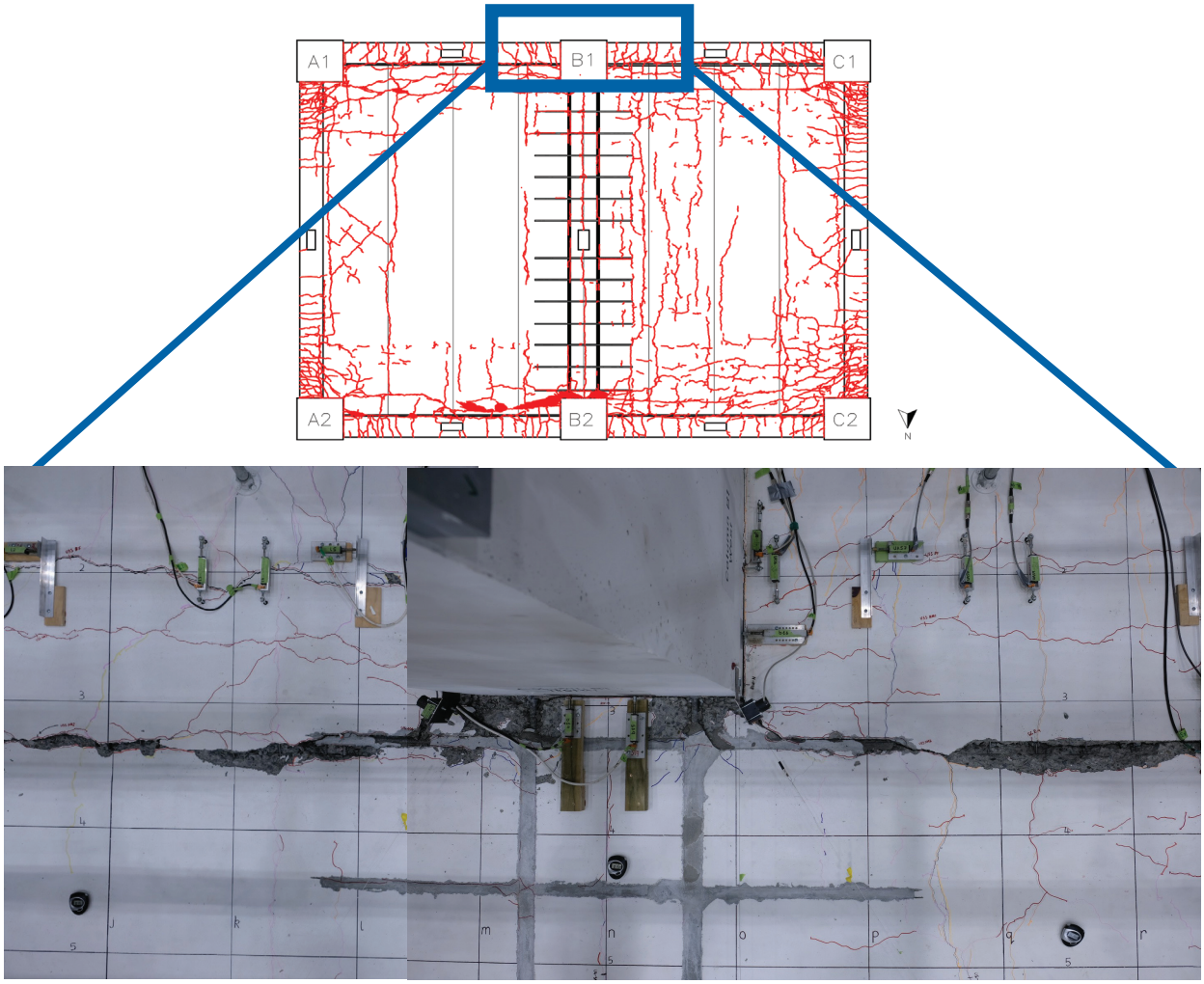

(a) Location on specimen and floor-column interface prior to rhomboid 4 loading

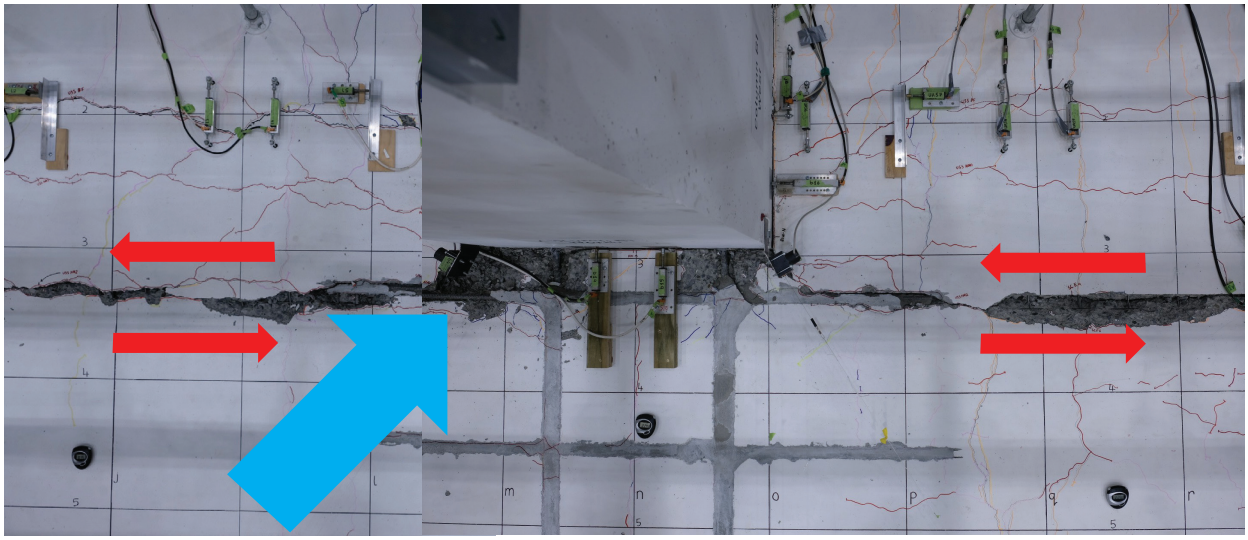

(b) Floor-Column interface with topping spalling at +0.25% floor plan shear distortion

The damage from these struts was likely more significant than for struts landing in the beams because it was the stiffest load-path. The compression strut load-path landing into beams was softened from needing to be transferred through the damaged beam plastic hinges.

Topping spalling from compression struts lands directly into column B2 was not observed. This was due to the split that developed between unit 5 and unit 6 in the positive direction removing and softening the diaphragm load-path directly into column B2.

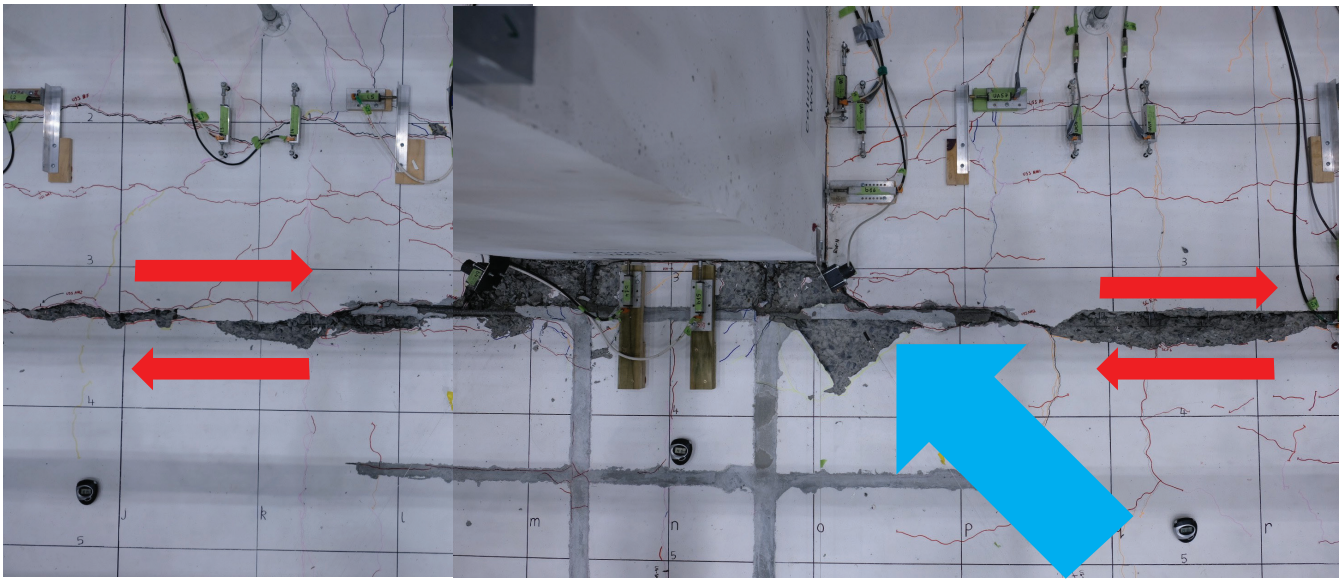

(c) Floor-column interface with topping spalling at -0.25% floor plan shear distortion

Figure 25: Evidence of compression struts landing directly into the B1 intermediate column at a high damage state due to contact stresses formed by tie-bar anchorage rubble

In both the TEST 1 and TEST 2 experiments, similar behaviour was observed with unit-unit interactions. As seen by the crack patterns displayed in Figure 14 and Figure 15, the intra-span units (units within the span, i.e. not alpha or beta units) and beta units acted as a single block rather than in a shear "racking" fashion that would have created significant cracking between each individual unit. Significant inter-unit cracking triggered in weak points within or adjacent to the alpha units and between or adjacent to the beta units. Once significant cracking was triggered at these weak points, additional damage concentrated at them instead of distributing between other unit interfaces. A likely cause for the ability of the intra-span units to act as a single element without significant damage was the relative flexibility of the beams once they began to twist. Warping and rotation of the beam plastic hinges was where deformation incompatibility demands between the intra-span units and support beams concentrated.

4 CONCLUSIONS

The previously described experimental observations have led to the following conclusions and recommendations related to precast floor units and floor diaphragms for practicing engineers:

- Residual floor diaphragm load-paths will exist even at high damage states with very wide cracks if there is a viable gravity load path for the floor and there is adequate continuity reinforcement. However there is high potential for designed strut-and-tie load-paths to break down across beta-unit-to-beta-unit interfaces where precast flooring systems are used due to local deformation incompatibility leading to mesh rupture. This is a particular concern where non-ductile mesh has been installed. Further research would be beneficial to determine if this issue still exists where ductile mesh has been installed. Based on the significant simultaneous tensile demands from the bowstring effect (described in Part II (Parr et al. 2022)) and vertical dislocation across the beta-beta unit interface, it is likely that significant strength improvement from the beta-unit-to-beta-unit stitching bars is required to prevent concentration of damage across this interface. Additionally, struts and ties can only reliably land in beams of the support frame and must be transferred into columns via the beam plastic hinge rather than landing directly into columns. For column faces of intermediate columns where tie-bars were anchored, struts were observed landing into the column face only after large amounts of damage had occurred to the floor topping.
- Contact stresses appear to form across wide concrete cracks in floors due to rubble replenishment. These contact stresses provide a rigid connection resistant to in-plane shear deformation that can allow diaphragm compressive struts to land on beams. Formation of aggregate rubble from local concrete crushing appears to be improved near steel reinforcing, particularly deformed rebar (but also mesh) as depicted in Figure 20 and Figure 26.

  This is likely due to bond with the bar causing substantial local cone-type cracking in the concrete when the steel bar deforms. Based on limited available test data presented herein, starter bar spacing of

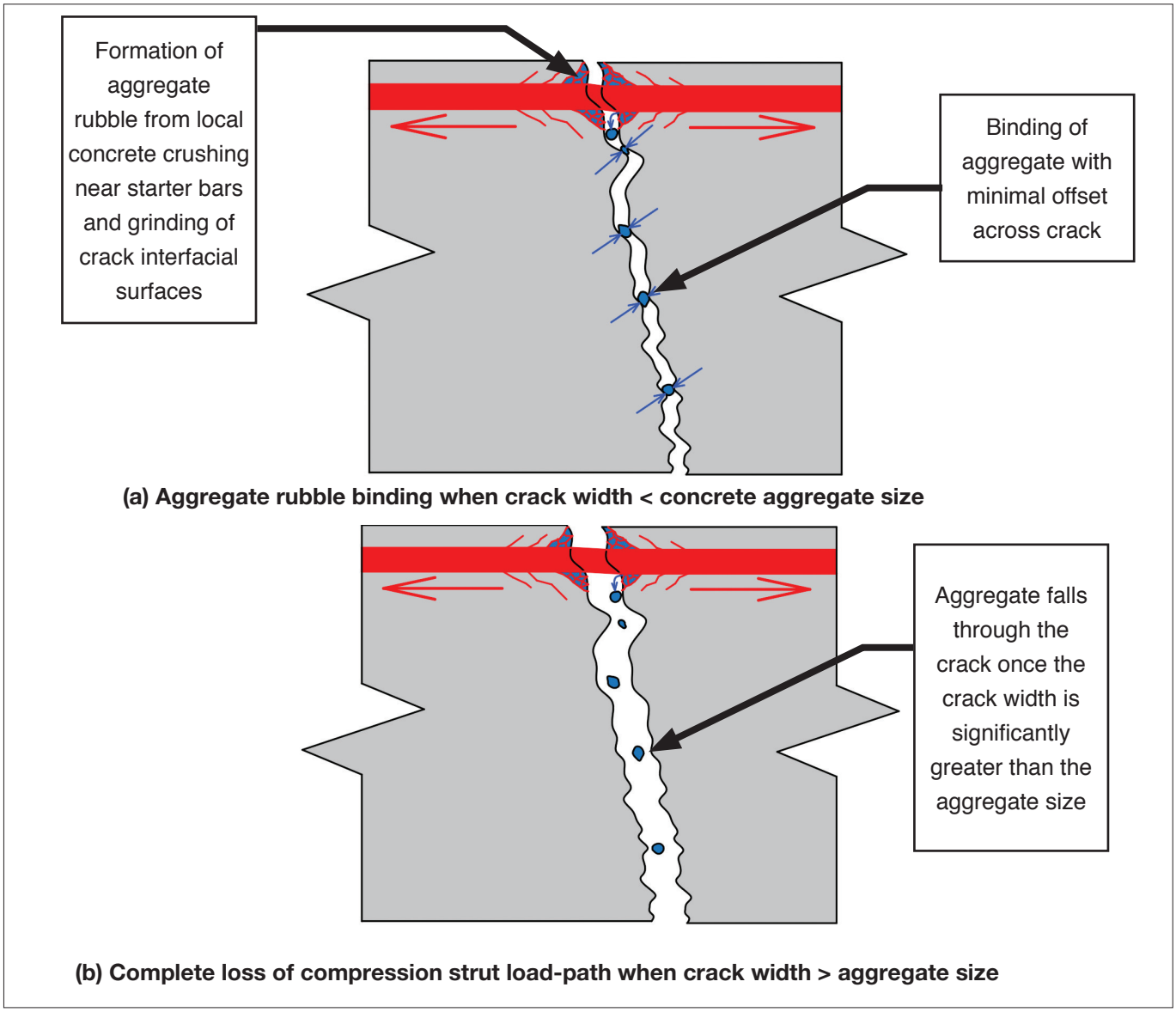

Figure 26: Residual compression strut load-paths forming across wide cracks due to aggregate rubble binding

400mm centre-to-centre crossing the crack interface appears to provide adequate rubble formation to transfer load across wide cracks. Smaller starter bar spacing should increase rubble formation, further ensuring a residual load-path develops. It is proposed that the maximum reliable crack width a compression strut can form across is dependent on the aggregate size used in the topping concrete mix. This is because aggregate rubble wedges itself between the crack interfaces and individual pieces of aggregate are unlikely to crush under compressive demands.

- Tie-bars are currently required between intermediate columns (with tie capacity to exceed 5% of maximum total axial compression force acting on the linked column or exceed 20% of the shear force from seismic actions in the column: Cl. 10.3.6 of NZS 3101:2006) to prevent them from bowing out of the structure which can lead to catastrophic floor failure. A secondary benefit of tie bars was observed during testing; that rubble is generated near the tie-bar anchor locations under earthquake loading due to bond stresses between the tie-bar and floor topping. However, this residual contact stress load path associated with the concrete around the column tie bars appears to require extensive damage and is only likely to develop after the building has experienced high peak drifts.
- For further analysis of the diaphragm performance observed in the super-assembly experiments conducted at the University of Canterbury in 2020 and 2021 refer to Part II (Parr et al. 2022)

5 REFERENCES

Brooke, N. (2022). "Overview of Retrofit Requirements and Techniques for Precast Concrete Floors." SESOC Journal, 35(1).

Büker, F., Brooke, N., Hogan, L., Elwood, K., Bull, D. and Sullivan, T. (2022). "Design Recommendations for Strongbacks Retrofits." SESOC Journal, 35(1).

Büker, F., Parr, M., De Francesco, G., Hogan, L., Bull, D., Elwood, K., Liu, A. and Sullivan, T. (2022). "Seismic Damage Observations of Precast Hollow-Core Floors From Two Full-Scale Super-Assembly Tests." SESOC Journal, 35(1).

Fenwick, R., Bull, D. and Gardiner, D. (2010). "Assessment of Hollow-core Floors for Seismic Performance (Research Report No. 2020-02; p. 152)."University of Canterbury, Christchurch, New Zealand.

Henry, R. and Ingham, J. (2012). "Performance of Precast Concrete Floor Systems During the 2010/2011 Canterbury Earthquakes." The New Zealand Concrete Industry Conference 2012 Hamilton.

Kam, W., Pampanin, S. and Elwood, K. (2011). "Seismic Performance of Reinforced Concrete Buildings in the 22 February Christchurch (Lyttelton) Earthquake." New Zealand Society for Earthquake Engineering (NZSEE).

Nievas, C. and Sullivan, T. (2017). "Accounting for Directionality as a Function of Structural Typology in Performance-Based Earthquake Engineering Design." Earthquake Engineering and Structural Dynamics, 46, 791-809.

Parr, M. (2022). "Retrofit Solutions for New Zealand Hollow-Core Floors and Investigation of True Floor Diaphragm Load Paths in Earthquakes." PhD, University of Canterbury, Christchurch, New Zealand - Currently in preparation.

Parr, M., Büker, F., De Francesco, G., Bull, D., Elwood, K., Hogan, L., Brooke, N., Liu, A. and Sullivan, T. (2022). "Load-Path and Stiffness Degradation of Floor Diaphragms in Reinforced Concrete Buildings Subjected to Lateral Loading – Part II, Data Analysis." SESOC Journal, 35(1).

Paulay, T. (1996). "Seismic Design of Concrete Structures - The Present Needs of Societies." Eleventh World Conference on Earthquake EngineeringAcapulco, Mexico.

SNZ (2017). "Concrete Structures Standard (Incorporating Amendment No. 1, 2 and 3). NZS3101.1:2006." Standards New Zealand (SNZ), Wellington, New Zealand.

Suzuki, T., Elwood, K., Puranam, A., Lee, H., Hsaio, F. and Hwang, S. (2020). "Seismic Response of Half-Scale Seven-Storey RC Systems with Torsional Irregularities: Blind Prediction." NZSEE 2020 Annual Conference, New Zealand Society for Earthquake Engineering (NZSEE).

EARTHQUAKE RESPONSE UNCERTAINTREE

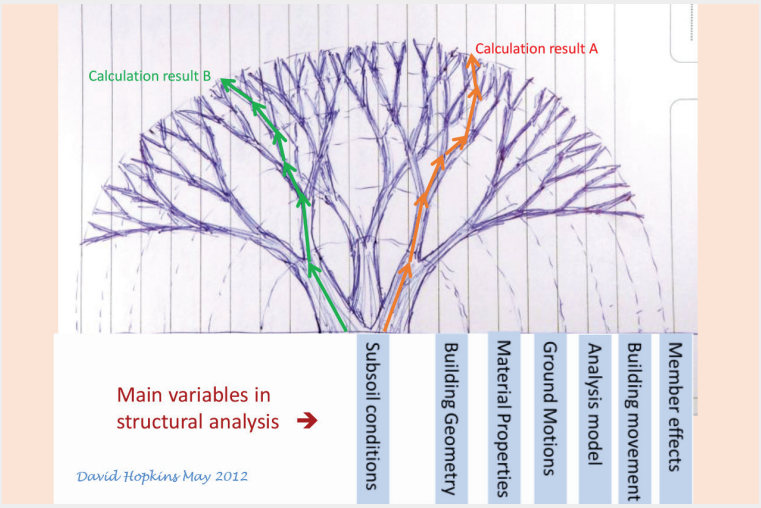

These and other examples, together with the challenges faced in the forensic time-history analyses of the CTV Building, led me to produce this ***Earthquake Response Uncertaintree***. This diagram reinforces the message that calculations, regardless of their sophistication, provide only estimates - not precise predictions. Analyses involve many assumptions, many of which are hidden from engineers' view within software. The implications of these assumptions need to be fully understood when making design decisions.

It is ***real structures, as designed and built***, that have to resist earthquake actions – not the theoretical models we analyse.

David Hopkins

ISSN No. 2744-7871